HEALTH AND MEDICINE

Near-infrared oxidative phosphorylation inhibitor integrates acute myeloid leukemia–targeted imaging and therapy

Chi Zhang[1]*, Tao Liu[1]*, Peng Luo[1]*, Li Gao[2], Xingyun Liao[1], Le Ma[1], Zhongyong Jiang[1], Dengqun Liu[1], Zeyu Yang[1], Qingzhi Jiang[1], Yu Wang[1], Xu Tan[1], Shenglin Luo[1†], Yang Wang[1†], Chunmeng Shi[1†]

Acute myeloid leukemia (AML) is a deadly hematological malignancy with frequent disease relapse. The biggest challenge for AML therapy is the lack of methods to target and kill the heterogeneous leukemia cells, which lead to disease relapse. Here, we describe a near-infrared (NIR) fluorescent dye, IR-26, which preferentially accumulates in the mitochondria of AML cells, depending on the hyperactive glycolysis of malignant cell, and simultaneously impairs oxidative phosphorylation (OXPHOS) to exert targeted therapeutic effects for AML cells. In particular, IR-26 also exhibits potential for real-time monitoring of AML cells with an in vivo flow cytometry (IVFC) system. Therefore, IR-26 represents a novel all-in-one agent for the integration of AML targeting, detection, and therapy, which may help to monitor disease progression and treatment responses, prevent unnecessary delays in administering upfront therapy, and improve therapeutic efficiency to the residual AML cells, which are responsible for disease relapse.

INTRODUCTION

Acute myeloid leukemia (AML) is a deadly hematological malignancy, comprising the genetically and morphologically heterogeneous groups of aggressive malignant cells (*1*, *2*). Although deep sequencing and recent molecular discoveries have provided tremendous insights into the underlying biology of AML, the long-term survival for AML patients is still unsatisfactory. This is due to the current treatment strategies failing to eliminate all malignant cells, which will eventually lead to disease relapse (*3*). Disease relapse is the most common cause of death in AML patients, and the lack of subsequent treatment strategies after relapse makes the cure of AML more challenging. Recent studies indicate the heterogeneous constitution of AML containing different types of leukemia cells with variable responses to chemotherapies. Among them, a rare population of residual chemotherapy-resistant leukemia cells is thought to drive the AML relapse after therapy (*4*, *5*). Techniques such as real-time quantitative polymerase chain reaction (qPCR) or multiparameter flow cytometry have been used to assess malignant cells in AML based on specific mutations, which have provided prognostic information for patient outcomes and profoundly affect clinical decision-making for disease management (*3*, *6*). However, most AML patients fail to present enough typical mutations for current detection due to genetic abnormal heterogeneity and genomic complexity (*7*, *8*). The residual leukemia cells are a rare population of cells responsible for reinitiating and maintaining disease, which are infeasible to be collected to enough events at the right time to evaluate valid disease information using current techniques. Therefore, developing new AML-targeting methods based on the common vulnerability of malignant cells is urgently needed to accurately detect and eliminate the heterogeneous malignant cells in AML patients. Especially, strategies combining targeted therapy with on-time treatment response monitoring and real-time detection of residual cells will help to prevent unnecessary delays in administering upfront therapy in AML, improve treatment efficiency, and reduce disease relapse (*9*, *10*). Thus, a new strategy simultaneously achieving malignant cells targeting detection and therapy is of particular significance in reducing AML relapse and is emerging as the next important direction for AML treatment.

Recently, studies on the fundamental roles of cellular metabolism reprogramming in tumor development and progression are given more emphasis (*11*). In particular, the increase of glycolysis even in the presence of oxygen, known as aerobic glycolysis, is reported as an important hallmark for cancer cells. AML is no exception to the general rule that increased glycolysis is the basic metabolic characteristic of leukemia cells, and hyperactive glycolysis is a common vulnerability for AML targeting and treatment (*12*). However, previous therapeutic strategies merely based on glycolytic inhibition fail to achieve satisfactory results in AML treatment. Treatment failure with glycolysis inhibitor occurs because increasing research studies have emphasized that, in addition to glycolysis, some tumors like brain cancer and AML depend more on enhanced mitochondria-specific oxidative phosphorylation (OXPHOS) for bioenergetic and biosynthetic processes (*13*). In particular, residual chemotherapy-resistant leukemia cells are demonstrated to show increased mitochondrial mass, retain active polarized mitochondria, and rely more on mitochondrial OXPHOS for survival (*14*). Therefore, current studies on the treatment vulnerability toward mitochondrial OXPHOS in leukemia cells are given more emphasis. Several strategies through inhibition of mitochondrial protein synthesis or inhibition of electron transport chain (ETC) complexes may hold great therapeutic potential in AML treatment (*13*, *15*, *16*). However, mitochondrion is the central checkpoint of cell metabolism and is involved in energetic and biosynthetic processes of cells; the integrity and functions of mitochondria are comparably important for almost all cells. The present application of OXPHOS inhibitors in anticancer therapy

[1]Institute of Rocket Force Medicine, State Key Laboratory of Trauma, Burns and Combined Injury, College of Preventive Medicine, Third Military Medical University (Army Medical University), Chongqing 400038, China. [2]Department of Hematology, Xinqiao Hospital, Third Military Medical University (Army Medical University), Chongqing 400037, China.
*These authors contributed equally to this work.
†Corresponding author. Email: shicm@sina.com (C.S.); 200616wy@163.com (Y.W.); luosl@tmmu.edu.cn (S.L.)

limits our understanding of mitochondria in cancer cells and the lack of tumor-targeting accumulation strategies, which may result in OXPHOS inhibitors not sufficiently reaching the tumors (*17*) and inducing unacceptable side effects, like neurotoxicity (*18*, *19*) and nausea/vomiting (*20*). Thus, the development of new strategies with both malignant cell targeting property and mitochondrial OXPHOS inhibiting ability would hold great therapeutic promise in improving AML treatment efficacy and reducing side effects. In previous work, we have synthesized a class of heptamethine cyanine dyes with structure-inherent near-infrared (NIR) fluorescence and solid tumor targeting ability (*21*, *22*). The heptamethine cyanine dyes are preferentially retained in the mitochondria of different kinds of solid tumor cells, relying on the hyperactivity of hypoxia-inducible factor–1α (HIF-1α)/glycolysis metabolism and the increase of SLCO1B3 transporter's activity in tumor cells (*23*–*25*). Because aerobic glycolysis is the basic metabolic characteristic of malignant cells and has profound effects on tumor genesis and progression, these dyes provide a new mechanism for tumor-targeting strategy based on the inherent functional properties of tumor cell metabolism. In this study, we aim to characterize a candidate NIR dye for hematological malignancy targeting and therapy by modifying with water-soluble amino acid ester groups in heptamethine cyanine dyes. Of the newly synthesized dyes, we have identified IR-26 as an all-in-one NIR dye for integrating AML targeting, detection, and therapy simultaneously. The newly designed IR-26 dye retains the preferential accumulation ability in the mitochondria of hematological malignant cells rather than normal cells depending on the same mechanism as in solid tumors. The water solubility of IR-26 is greatly improved by inhibiting the intermolecular hydrogen bond formation, which would decrease J1 aggregates and the serum protein binding rate of IR-26, favoring hematological malignant cell targeting. IR-26 also has the NIR fluorescent ability with the absorption and emission peak in the range of 700 to 900 nm, which has great advantages for cancer cell imaging with deep tissue penetration and low-background autofluorescent interference (*26*, *27*). Therefore, IR-26 is demonstrated to dynamically detect the circulating malignant cells in vivo in a noninvasive way using a NIR in vivo flow cytometry (IVFC) system established previously (*28*), which holds significance in continuously monitoring of disease progression, treatment responses, and disease relapse. IR-26 is demonstrated to target the ETC proteins, SDHA, and ATP5B and inhibit the complex II and complex V activities to impair mitochondrial OXPHOS functions, resulting in increased apoptosis in AML cells. IR-26 exerts its excellent therapeutic efficiency in AML by selectively inhibiting the leukemia cell population and prolonging the survival of AML mice without inducing obvious side effects. Overall, our work may provide an entirely new mechanism for AML targeting based on the hyperactive glycolytic metabolism of malignant cells and a rational therapeutic strategy for integrating AML targeting, detection, and treatment by a glycolysis-dependent mitochondrial OXPHOS inhibitor, IR-26, which indicates a new opportunity to improve AML clinical treatment efficiency and reduce disease relapse.

RESULTS

Synthesis and characterization of AML-targeted dye

On the basis of previous structure-activity studies, we have characterized that heptamethine core with lipophilic cationic property is essential for tumor targeting in heptamethine cyanine dyes (*29*, *30*). In this study, we have synthesized a series of derivatives by modifying with various *N*-alkyl side chains on the heptamethine core to obtain new dyes that target AML cells. Eight candidate mitochondria-targeted dyes were chosen to study their AML cell-targeting properties. As shown in fig. S1A, IR-26 exhibited the highest NIR fluorescence contrast index values when compared with other dyes, suggesting a good preferential accumulation ability to AML cells. Moreover, IR-26 showed the highest cytotoxicity in AML cells (fig. S1B), with a half-maximal inhibitory concentration (IC_{50}) of only 2.660 μM. The synthetic route and chemical structure of IR-26 are shown in fig. S2 and Fig. 1A. The absorption and fluorescence spectra of IR-26 were investigated in methanol (MeOH), 10% fetal bovine serum (FBS), and phosphate-buffered saline (PBS; Fig. 1, B and C) and indicated that the absorption and emission peak of IR-26 were in the NIR region (700 to 900 nm). IR-26 showed good stability in 10% serum and was easy to disperse in the PBS solution without disturbing serum albumin (fig. S3). All these features make IR-26 a promising NIR dye for hematological malignancy biomedical imaging. Then, human AML cells, HL-60, or peripheral blood mononuclear cells (PBMCs) were incubated with IR-26 at similar conditions; cellular NIR fluorescence was detected by confocal microscopy. Figure 1D shows that IR-26 accumulated in HL-60 cells increasingly in a time-dependent manner, indicating its preferential accumulation ability in AML cells. This AML-targeted property was also observed in different types of AML cell lines (HL-60, NB4, and THP-1; Fig. 1E) when compared with the normal PBMCs. Last, athymic nude mice with green fluorescent protein (GFP)–labeled HL-60 (lentiviral transfection) tumor xenografts at subcutaneous spaces were imaged after a single administration of IR-26 at 0.2 mg/kg through intravenous injection. Figure 1F and fig. S4A show that intense NIR signals can be clearly visualized, associated with the implanted GFP-labeled HL-60 tumor sites using Kodak In-Vivo Imaging System FX Pro. Histopathologic analysis of tumor frozen section indicated that NIR fluorescence was colocalized with GFP fluorescence in cancer cells (fig. S4B), further demonstrating the preferential accumulation of IR-26 in AML cells. Thus, IR-26 may be a promising NIR dye for hematological malignancy targeting and biomedical imaging based on our results.

Specificity of IR-26 for AML cell detection

To further investigate whether the leukemia-targeted IR-26 could be used to detect AML cells in peripheral blood, PBMCs and pre-established GFP-labeled HL-60 cells were mixed to mimic the complex cellular components in peripheral blood and incubated with 5 μM IR-26 under 37°C. Then, the mixed cells were detected using flow cytometry, and the results showed that IR-26 could easily distinguish the HL-60 cells from PBMCs by NIR fluorescence (Fig. 2A). IR-26 could recognize the same population of leukemia cells as GFP-labeled cells in the mixed cells (Fig. 2, B and C) with a good accuracy in targeting AML cells. Under confocal microscopy, all GFP-labeled AML cells could be detected by IR-26 (Fig. 2D). The NIR fluorescent cell population was a little bigger than the GFP fluorescent cell population (Fig. 2E), indicating a better sensitivity of NIR fluorescent dye in AML cell detection than GFP. Impressively, IR-26 could also be used to detect AML cells from clinical patients when compared with PBMCs from healthy donor (Fig. 2F). To further investigate the detection property of IR-26 in leukemia cells in vivo, a mouse model of human AML was established by intravenous injection of GFP-labeled human AML cells into sublethally irradiated C57BL/6 mice (Fig. 2G). Histological examination and immunohistochemistry assay revealed that extensive infiltration of GFP-labeled

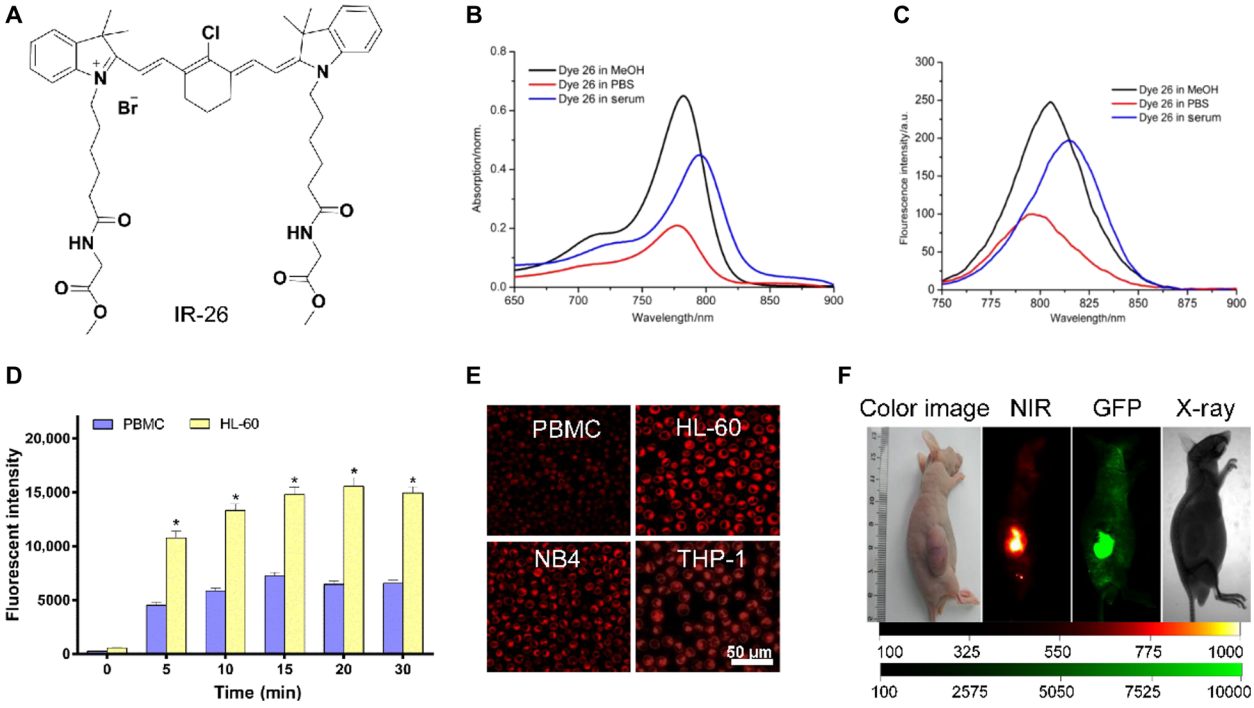

Fig. 1. Identification of NIR dye for leukemia cell targeting. (**A**) Chemical structure of IR-26. (**B**) Absorption spectra of 2 μM IR-26 in 10% FBS, methanol (MeOH), and PBS. (**C**) Fluorescence emission spectra of IR-26 in 10% FBS, methanol (MeOH), and PBS. a.u., arbitrary units. (**D**) NIR fluorescence intensity in human peripheral blood mononuclear cells (PBMCs) and HL-60 cells was compared after incubation with the same concentration of IR-26 for various times ($n = 3$). MitoTracker Green was used to avoid the impact of cell size in comparing fluorescence of PBMCs to AML cells. (**E**) PBMCs and AML cell lines (HL-60, NB4, and THP-1) were incubated with IR-26 for the same condition and imaged by a laser confocal scanning microscope (Leica) with 633-nm excitation. (**F**) Preferential accumulation of IR-26 in athymic tumor-bearing nude mice preestablished with GFP-labeled HL-60 tumor xenografts. The animals were subjected to fluorescence imaging and x-ray imaging using Kodak In-Vivo Imaging System FX Pro (New Haven, CT). Photo credit: Tao Liu, Institute of Rocket Force Medicine, Third Military Medical University. Error bars denote means ± SD. *$P < 0.05$.

leukemia blast cells was shown in the hematopoietic organs (fig. S5, A and B), and the spleens from the transplantation group were much heavier than those from the control group (fig. S5C). In addition, we have established a NIR IVFC that treats blood flow as the natural sheath flow for tracking of specific cells in the circulatory system noninvasively. The IVFC was used to observe, in the long term, GFP fluorescent cells in animal peripheral blood and showed that GFP-labeled HL-60 cells continuously existed in the circulatory system of transplanted mouse for more than 20 days (fig. S5D), further confirming the stability of AML animal models. To test whether IR-26 could be used to monitor AML cells in real time, the dual-channel (GFP and NIR fluorescence) IVFC was used to detect the NIR fluorescent leukemia cells in vivo after mice were intravenously injected with IR-26 (0.2 mg/kg), with GFP fluorescence as the internal reference of GFP-labeled HL-60 cells. Figure 2H shows a representative data trace of leukemia cells with both GFP and NIR fluorescence signal in the AML animal model, indicating that IR-26 could be used to specifically detect AML cells in vivo using the IVFC system. After 10 min of detection, the number of peaks per minute in GFP channel, NIR channel, or dual channel showed no statistical significance (Fig. 2I), suggesting the good sensitivity and accuracy of IR-26 in detecting AML cells in vivo. To further validate the leukemia targeting property of IR-26 in vivo, bone marrow, spleen frozen section, and peripheral blood were detected by confocal microscopy after mice were sacrificed. As shown in Fig. 2J, the NIR fluorescence signal overlapped with GFP-labeled leukemia cells in all these organs, which confirmed the targeting and detection property of IR-26 in AML cells. Last, we studied the indicated mechanisms for the leukemia-targeting property of IR-26. As shown in fig. S6A, inhibition of cellular glycolysis by 150 mM 2-deoxy-D-glucose or inhibition of SLCO1B3 transporter's activity by 250 μM sulfobromophthalein reduced the uptake of IR-26 in AML cells, which was similar to our previous studies in solid tumor targeting. In addition, the cellular level of HIF-1α was also demonstrated to be responsible for the preferential uptake of IR-26 in leukemia cells (fig. S6B). We further observed that the expression of SLCO1B3 was positively correlated with HIF-1α level in AML cells (fig. S6C). The expression of SLCO1B3 was also demonstrated to be up-regulated in AML patients (fig. S6, D and E), which was analyzed from the public data GSE9476. In conclusion, IR-26 was demonstrated to directly target AML cells based on the hyperactivity of HIF-1α/glycolysis metabolism and increased SLCO1B3 transporter's activity in leukemia cells, which was similar to the previous targeting mechanism in solid tumors (*23*). This entirely new AML-targeting mechanism may greatly help to improve AML treatment strategy in disease detection and therapy.

Selective killing effects of IR-26 in AML cells

In consideration of the AML targeting and detection property of IR-26, further investigation of anti-leukemia effects of IR-26 may help to improve AML treatment strategies by integrating AML continuous detection and targeted treatment. IR-26 showed the highest cytotoxicity for AML cells among the eight candidate dyes. Further

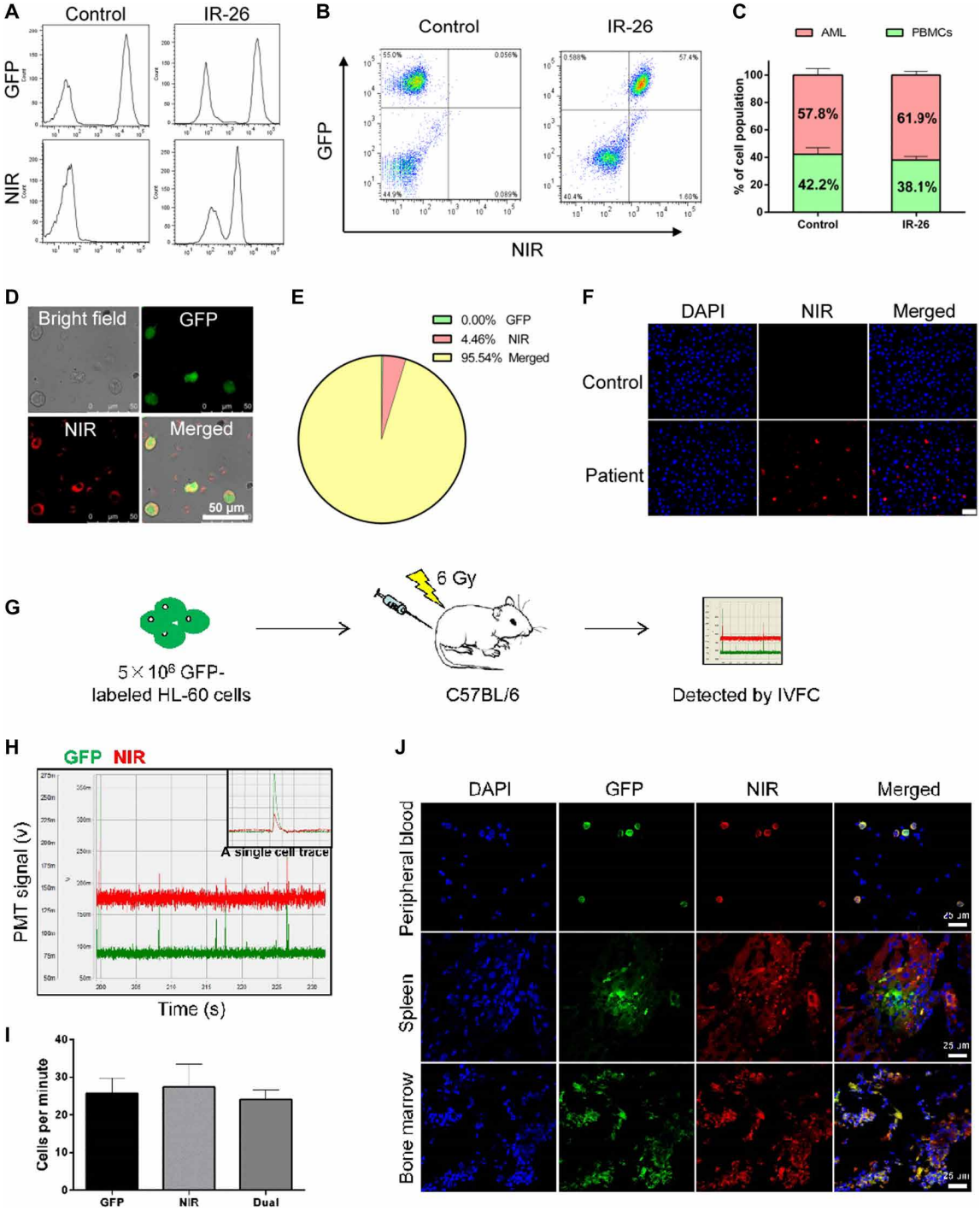

Fig. 2. Specificity of IR-26 for AML cell detection. (**A**) Flow cytometry (BD FACSVerse, BD Biosciences) analysis of the AML-targeting property of IR-26 in PBMCs and GFP-labeled HL-60 mixed cells; NIR fluorescence was detected with 633-nm excitation and 780-nm emission after mixed cells were incubated with IR-26 or PBS. (**B** and **C**) Flow cytometry analyzing the accuracy of IR-26 in targeting the GFP-labeled leukemia cell population in the mixed cells. (**D**) Confocal microscope detected the colocalization of NIR fluorescence with GFP fluorescence after the mixed cells were incubated with IR-26. (**E**) Pie chart showing a better sensitivity of NIR fluorescent dye in detecting AML cells than GFP fluorescence. (**F**) Colocalization of IR-26 with AML cells in the clinical AML patient sample after incubation with 5 μM IR-26 for 20 min. Images were obtained using a confocal microscope (Leica) with 633-nm excitation. Nuclei were stained with Hoechst (blue). (**G**) Schematic representation of the experimental design (see also Materials and Methods) for AML cell detection in vivo by IR-26. (**H**) Data showing fluorescence peaks in IVFC of GFP channel (green) and IR-26 channel (red) and representative dual positive peak in both channels, indicating the accurate tracing of GFP-labeled AML cells in peripheral blood. (**I**) Statistical histogram showing the number of peaks per minute in the GFP channel, the NIR channel, and the dual channel detected using IVFC in peripheral blood of AML mouse model ($P > 0.05$). (**J**) Histopathologic analysis of peripheral blood, spleen, and bone marrow frozen sections of the AML mouse model by confocal microscope. Nuclei were stained with 4′,6-diamidino-2-phenylindole (DAPI; blue). Error bars denote means ± SD.

studies indicated that IR-26 effectively killed different types of AML cell lines (HL-60 and THP-1) in a concentration-dependent manner, with IC_{50} values of 2.629 and 2.351 μM, respectively (Fig. 3A). Western blot analysis indicated that IR-26 induced mitochondrial apoptosis in HL-60 and THP-1 cells by inducing PARP [poly(adenosine diphosphate–ribose) polymerase], caspase-3, and caspase-9 cleavages (Fig. 3B). Annexin V and propidium iodide (PI) staining by flow cytometry detection also indicated that IR-26 induced apoptosis in AML cells (Fig. 3C). To examine the potency of IR-26, which is widely used across species, the response of IR-26 to mouse and human leukemia cell lines (C1498, P388D1, HL-60, and THP-1) was assessed using oxygen consumption rate (OCR) and galactose viability assay. Figure S7 showed that IR-26 was similarly active in mouse (average IC_{50} = 4.788 μM) and human cells (average IC_{50} = 2.913 μM). Then, the cytotoxicity of IR-26 on AML cells and normal PBMCs was compared, and Fig. 3D shows that IR-26 induced HL-60 cell death with no obvious cytotoxic effects on human hematopoietic stem cells (HSCs), suggesting the targeted killing effects of IR-26 on AML cells. Moreover, IR-26 was also demonstrated to inhibit cell colony formation in HL-60 cells (Fig. 3E) and decreased the $CD34^+CD38^-$ subset of HL-60 cells with the increase of IR-26 (Fig. 3F), suggesting the inhibition effects of IR-26 on AML stem-like cells, which are responsible for chemotherapy resistance in AML. In summary, these studies indicated that IR-26 selectively induced apoptosis in AML cells and even in chemotherapy-resistant subset of cells, while the concentrations that appear pharmacologically achievable did not have similar negative effects on normal cells.

Anti-leukemia efficacy of IR-26 in AML mouse models

To further assess the anti-leukemia treatment effects of IR-26 in vivo, two AML mouse models were established and used. First, the AML xenograft mouse models were established by subcutaneous injection of HL-60 cells in the nude mice. After tumors became palpable, the mice were randomly divided into three groups and received intraperitoneal injection of PBS, cytarabine (50 mg/kg), and IR-26 (5.0 mg/kg). As shown in Fig. 4A, a distinct inhibition of tumor growth was observed after IR-26 treatment, while the treatment effect of cytarabine was limited. Tumor weight, which was measured after mice sacrifice, also indicated the marked anti-leukemia effect of IR-26 in vivo (Fig. 4B). Compared with the control group, IR-26

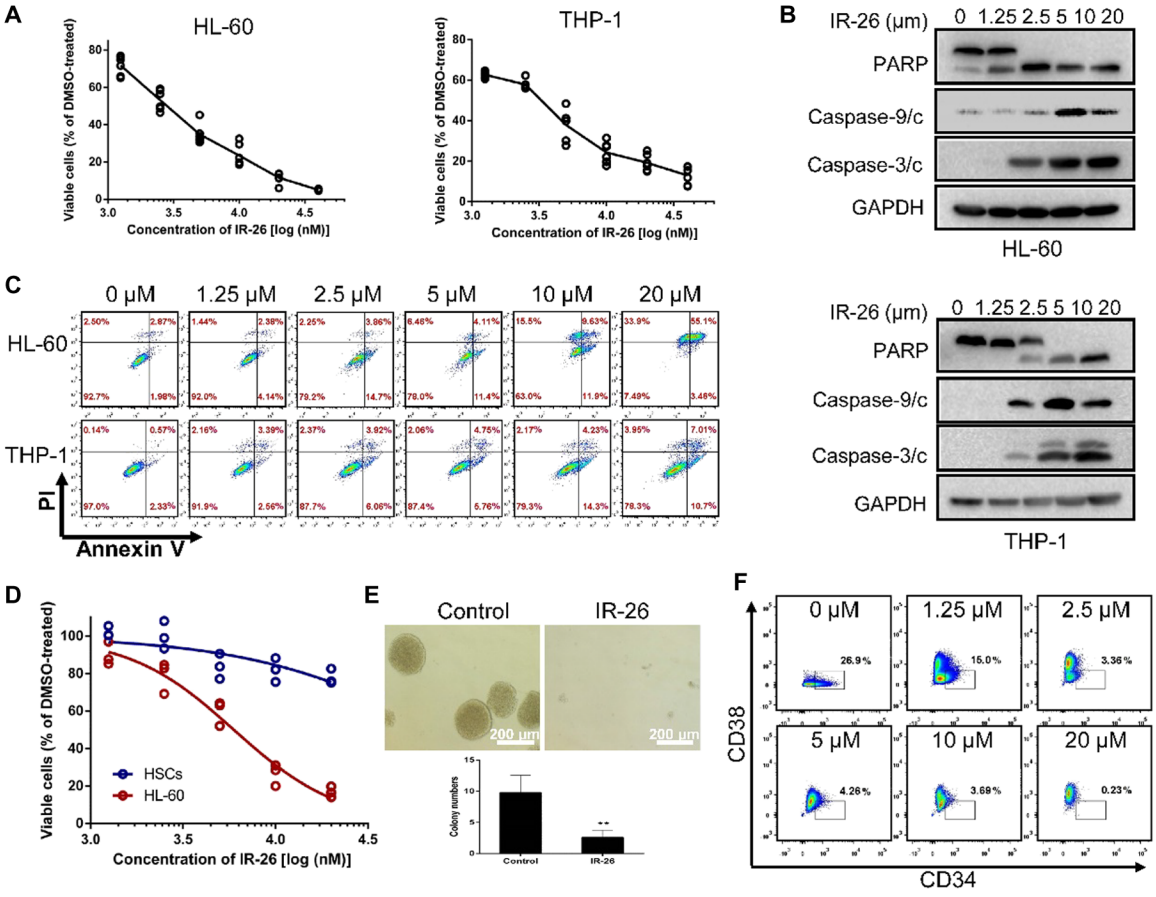

Fig. 3. IR-26 selectively kills AML cells in vitro. (**A**) Human AML cell lines (HL-60 and THP-1) were treated with various concentrations of IR-26 for 48 hours, and IC_{50} values were calculated. (**B**) HL-60 and THP-1 cells were treated with various concentrations of IR-26, and apoptosis-related markers were detected using Western blot. Glyceraldehyde-3-phosphate dehydrogenase (GAPDH) was taken as the loading control. (**C**) HL-60 and THP-1 cells were treated with IR-26 for 24 hours and stained with annexin V/PI to detect cell apoptosis by flow cytometry. (**D**) HL-60 cells and human hematopoietic stem cells (HSCs) were treated with different concentrations of IR-26 for 48 hours, and cell viability was measured and compared. (**E**) HL-60 cells were treated with IR-26 (5 μM) or dimethyl sulfoxide (DMSO) for 6 hours; 800 cells per well were seeded in the methylcellulose medium and cultured for 2 weeks; cells colonies were imaged and counted under inverted microscope. (**F**) Flow cytometry analysis and percentage of $CD34^+CD38^-$ cell subset after HL-60 cells were treated with different concentrations of IR-26. Error bars denote means ± SD. $^{**}P < 0.01$.

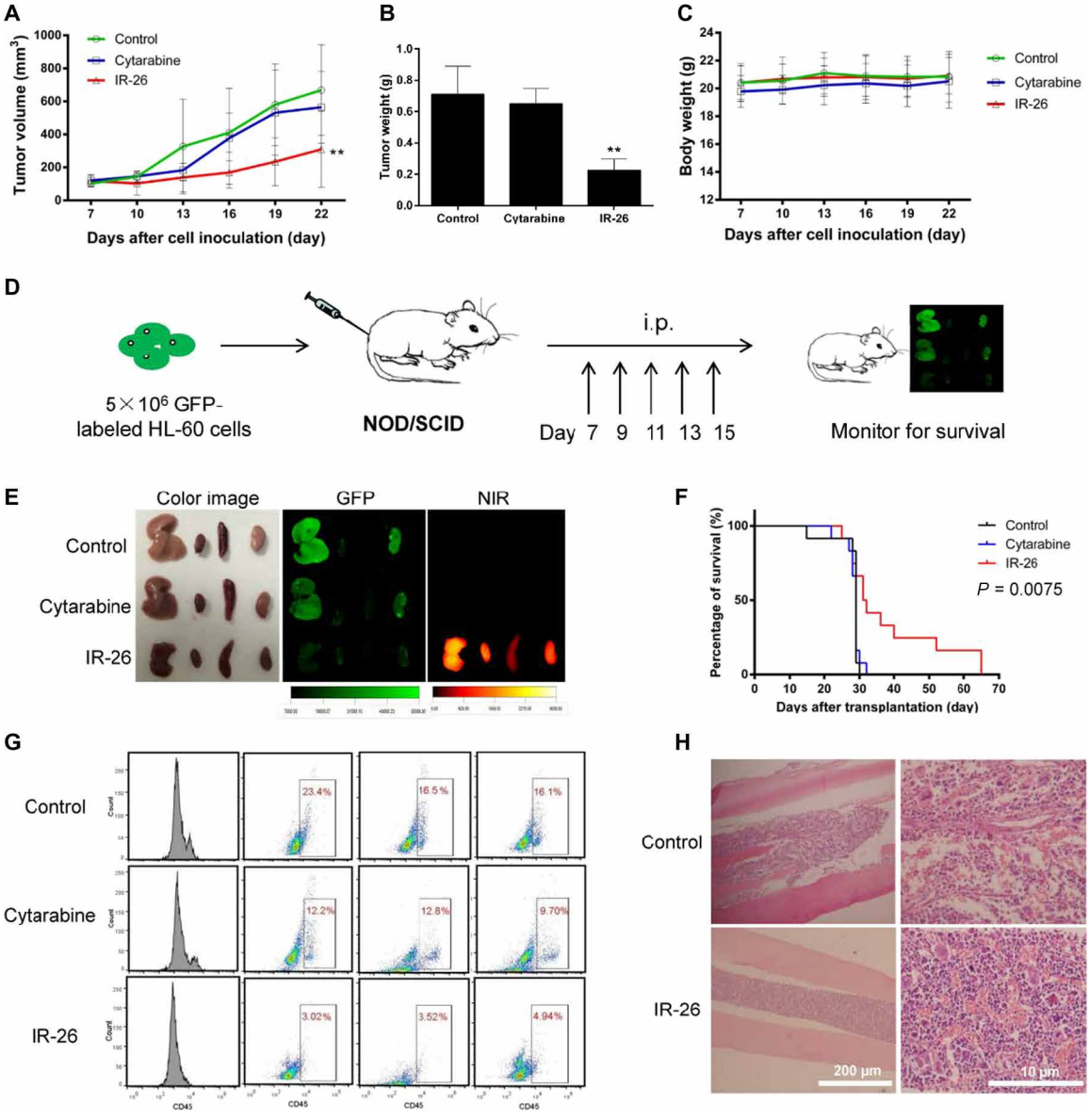

Fig. 4. Anti-leukemia effects of IR-26 in AML mouse models. (**A**) IR-26 effectively inhibits tumor growth in nude mice inoculated with HL-60 cells. Mice were treated with IR-26 (5 mg/kg every third day by intraperitoneal injection), cytarabine (50 mg/kg), or vehicle control; tumor volumes were calculated as length × (width)^2/2. $n = 5$, $^{**}P < 0.01$ compared with the control group. (**B**) Tumor weights of mice were measured and compared ($n = 5$, $^{**}P < 0.01$ compared with the control group). (**C**) Mice body weights were measured and compared ($n = 5$). (**D**) Schematic representation of the experimental design (see also in Materials and Methods) for anti-leukemia assay in mouse model, which is established by intravenous injection of GFP-labeled HL-60 cells into NOD/SCID mice. Mice were intraperitoneally (i.p.) injected with IR-26 (5 mg/kg), cytarabine (50 mg/kg), or PBS as vehicle control. (**E**) Detached liver, heart, spleen, and kidney were subjected to GFP and NIR imaging at day 25 after treatment, indicating a distinct decrease of GFP-labeled AML cells in IR-26–treated mice. Photo credit: Yang Wang, Institute of Rocket Force Medicine, Third Military Medical University. (**F**) Kaplan-Meier curve analysis demonstrated a survival advantage for mice treated with IR-26 ($n = 12$, $P = 0.0075$). (**G**) Chimerism of human HL-60 cells in the mouse bone marrow was quantified and compared by detecting cells that express human CD45 at day 25. (**H**) Pathologic analysis of bow marrow morphologic information in control and IR-26–treated mouse. Error bars denote means ± SD.

treatment did not cause body weight change (Fig. 4C) and obvious pathologic changes in vital organs (fig. S8), indicating its satisfactory safety for in vivo treatment. To evaluate the anti-leukemia effects of IR-26 at different doses, nude mice bearing HL-60 subcutaneous xenografts received IR-26 at doses of 0, 1, 3, or 5 mg/kg intraperitoneally. Figure S9 indicated that treatment with IR-26 at doses of 1, 3, and 5 mg/kg were all effective and led to significant tumor regression with no obvious body weight loss. Moreover, nonobese diabetic/severe combined immunodeficient (NOD/SCID) mice were engrafted with GFP-labeled human AML cells HL-60 by tail vein injection to establish orthotopic AML mouse model. One week after primary transplant of GFP-labeled AML cells, mice were treated with cytarabine (50 mg/kg) or IR-26 (5.0 mg/kg) every other day by intraperitoneal injection for five times (Fig. 4D; $n = 12$). At day 25, Kodak In-Vivo Imaging System FX Pro showed that dissected organs from IR-26–treated group displayed no obvious GFP fluorescence, while organs

from other groups showed strong GFP fluorescence (Fig. 4E), suggesting that nearly all GFP-labeled AML cells disappeared after mice were treated with IR-26. Moreover, IR-26 markedly prolonged the median survival of mice in Kaplan-Meier analysis when compared with the cytarabine-treated group (Fig. 4F; $P = 0.0075$). IR-26 treatment remarkably reduced tumor burden, manifested with a prominent decrease in percentage of $hCD45^+$ cells in the bone marrow (Fig. 4G). Hematoxylin and eosin staining revealed significantly reduced infiltration of leukemic cells and increased preservation of normal tissue structures in the bone marrow and other organs of mice treated with IR-26 when compared with the control group mice (Fig. 4H and fig. S10). The pharmacokinetic profiles are important for drug effectiveness and biosafety. The blood curve of IR-26 was also determined after intraperitoneal injection at a dose of 5 mg/kg (fig. S11), and the pharmacokinetic parameters were calculated ($t_{1/2}$ = 56.43 ± 6.38 hours, C_{max} = 115.23 ± 6.73 μg/liter, T_{max} = 4 ± 1.73 hours).

Disruption effects of IR-26 in mitochondrial metabolism

Because of the effective therapeutic benefits of IR-26 in AML, further investigation of the underlying mechanisms of IR-26–induced cell death is needed. Our previous studies have indicated that this kind of lipophilic cationic heptamethine dyes is more ready to reach a higher concentration in mitochondria due to the negative charge (*21*), and some mitochondrial membrane transporters may also help to transport into mitochondria (*25*). A subcellular location assay was performed, and it indicated that IR-26 specifically accumulated in the mitochondria of AML cells by colocalization with the mitochondria-specific probe MitoTracker Green (Fig. 5A). Moreover, transmission electron microscopy showed that IR-26 treatment induced mitochondria swelling and vacuolation in AML cells (Fig. 5B). IR-26 treatment also decreased mitochondrial membrane potential in AML cells (Fig. 5C). All these mitochondrial changes after IR-26 treatment suggested that mitochondria might be an important therapeutic target of IR-26. Our data further showed that IR-26 treatment increased mitochondrial reactive oxygen species (ROS) production in AML cells (Fig. 5D), and the mitochondrial ROS-specific scavenger MitoTEMPO significantly reversed IR-26–induced ROS production and cell death (Fig. 5E). Real-time analysis of mitochondrial respiration profiles using a seahorse XF96 analyzer indicated that IR-26 reduced the basal mitochondrial OCRs and the maximal respiration of mitochondria in HL-60 cells (Fig. 5F). In addition, the adenosine

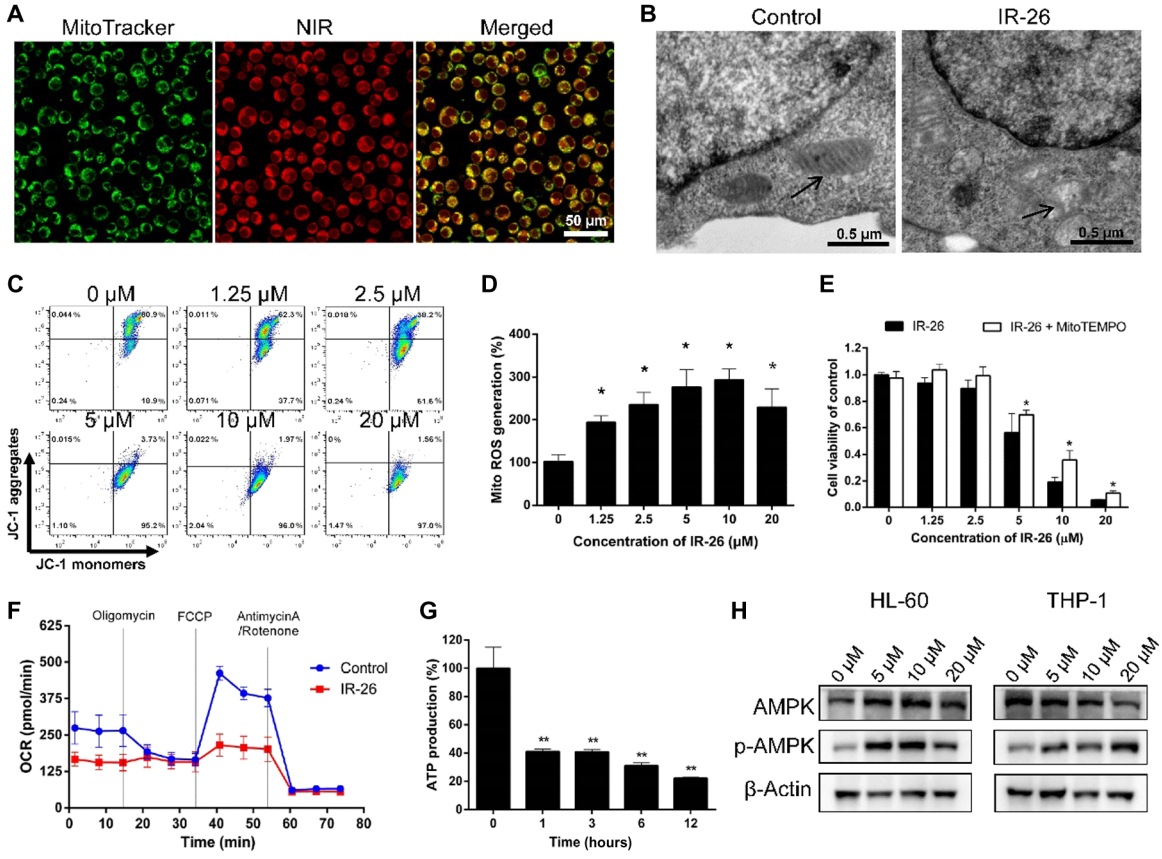

Fig. 5. Disruption effects of IR-26 in mitochondria of AML cells. (**A**) Specific accumulation of IR-26 in the mitochondria of HL-60 cells by colocalization with the mitochondria-specific probe (MitoTracker Green). (**B**) Transmission electron microscopy observation of mitochondrial morphologies in HL-60 cells. Black arrow indicates mitochondria. (**C**) Mitochondrial membrane potential was evaluated by the JC-1 aggregate/monomer fluorescence ratio in HL-60 cells. (**D**) Mitochondrial ROS productions in HL-60 cells were detected using MitoSOX (Invitrogen, Carlsbad, CA) after cells were treated with IR-26 for 1 hour ($n = 3$). (**E**) HL-60 cell viabilities were detected after cells were treated with increasing concentrations of IR-26 in the presence or absence of the mitochondrial ROS-specific inhibitor MitoTEMPO. (**F**) Real-time analysis of mitochondrial respiration profile of HL-60 cells using a seahorse XF96 analyzer after cells were treated with 10 μM IR-26 for 1 hour. (**G**) HL-60 cells ATP production were detected after treatment with 10 μM IR-26 for different times. (**H**) Western blot analysis of the energy metabolism regulating protein and AMPK signaling expression in HL-60 and THP-1 cells after treatment with different concentrations of IR-26. Error bars denote means ± SD. *$P < 0.05$ and **$P < 0.01$.

triphosphate (ATP) production was significantly decreased after cells were treated with increasing concentrations of IR-26 (Fig. 5G). These data suggested that mitochondrial OXPHOS of AML cells was markedly destroyed by IR-26 treatment. The adenosine monophosphate–active protein kinase (AMPK) is a key susceptor in the regulation of energy metabolism. IR-26 treatment significantly increased phospho-AMPK in AML cells, indicating the activated AMPK signaling in response to OXPHOS inhibition (Fig. 5H). All these data indicate that mitochondria are the important therapeutic target of IR-26, and directly impairing mitochondrial OXPHOS functions is the key mechanism of IR-26 to induce cell death in AML.

Molecular target of IR-26 in mitochondrial respiratory chain

To further explore the molecular mechanism through which IR-26 disrupts mitochondrial functions and OXPHOS in AML cells, metabolomic and molecular target analyses were performed in IR-26–treated HL-60 cells. First, HL-60 cells were treated with different concentrations of IR-26 for 12 hours, and cell lysates were subjected to TSQ Quantiva (Thermo Fisher Scientific, CA) analysis to measure metabolites from central carbon metabolism. Figure 6A shows that IR-26 treatment elevated the level of mitochondrial complex II substrate, succinate, but reduced the levels of downstream metabolites, fumarate and malate, in the tricarboxylic acid (TCA) cycle. These changes are consistent with mitochondrial complex II activity inhibition. Moreover, after HL-60 cells were treated with different concentrations of IR-26, all activities of mitochondrial respiratory chain complexes were detected using a MitoTox OXPHOS complex activity assay kit (Abcam), indicating that complex II and complex V activities were distinctly inhibited by IR-26 treatment (Fig. 6B). We then identified the potential interactive proteins of mitochondrial respiratory chain with IR-26 using a previously established method (*31*) and indicated that SDHA and ATP5B might be the interactive proteins of IR-26. The pull-down assay using the specific antibodies of SDHA and ATP5B further determined that IR-26 interacted with complex II and complex V proteins, SDHA and ATP5B (Fig. 6C). Therefore, the data suggested that IR-26 directly targeted the mitochondrial ETC proteins SDHA and ATP5B to inhibit complex II and complex V activities and disturbed mitochondrial OXPHOS functions to induce targeted killing effects in AML cells.

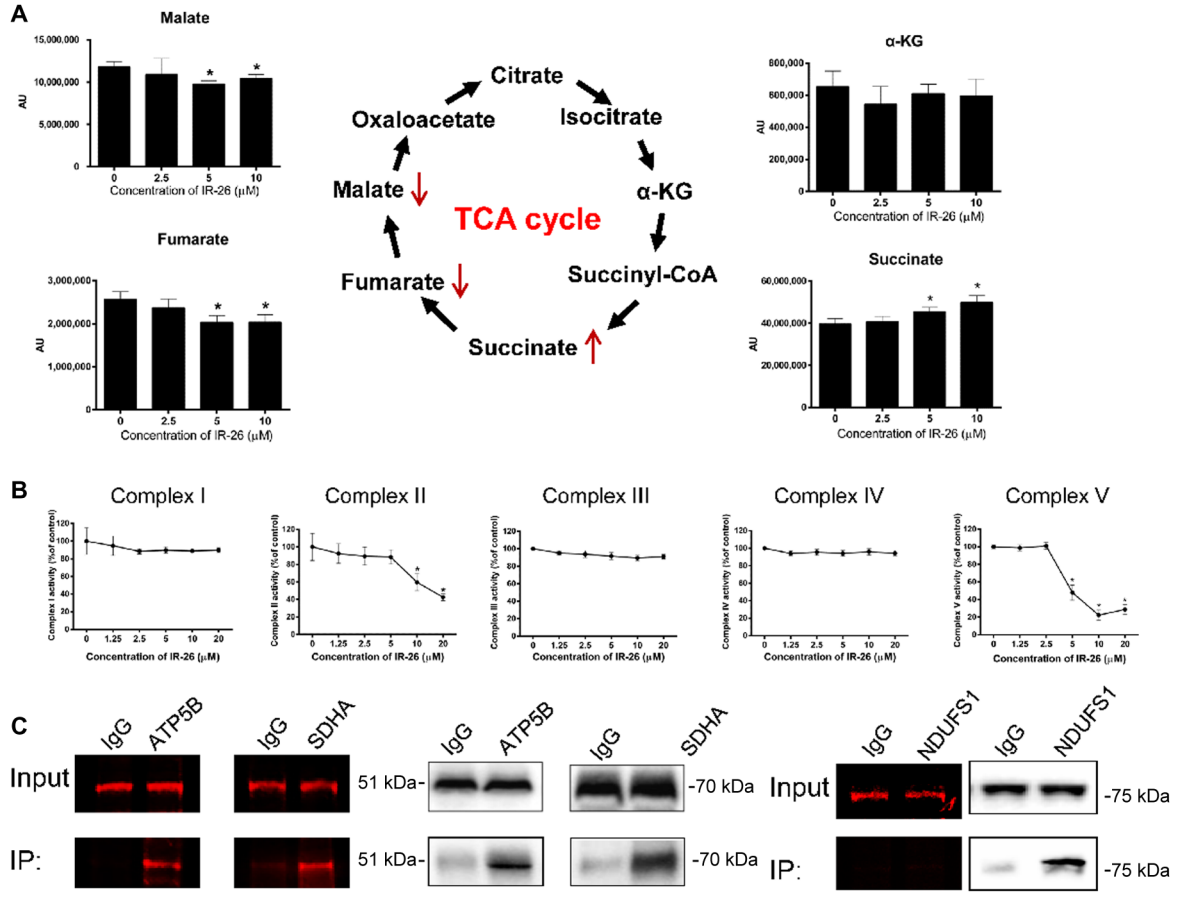

Fig. 6. IR-26 targets mitochondrial respiratory chain proteins in AML cells. (**A**) After treatment with different concentrations of IR-26, HL-60 cell lysates were subjected to TSQ Quantiva (Thermo Fisher Scientific, CA) analysis to measure the metabolites from tricarboxylic acid (TCA) cycle and the levels of TCA cycle intermediates, α-ketoglutarate (α-KG), succinate, fumarate, and malate after treatment with IR-26. AU, arbitrary units; CoA, coenzyme A. (**B**) Mitochondrial complex activities were measured after treatment with IR-26 using a commercially available kit (Abcam). (**C**) Pull-down assay was performed using mitochondrial protein ATP5B, SDHA, and NDUFS1 antibodies in IR-26–treated cancer cell lysates, showing that ATP5B and SDHA antibodies pulled down proteins with NIR fluorescence, but NDUFS1 antibody pulled down proteins with no NIR fluorescence, indicating that IR-26 directly targets mitochondrial proteins ATP5B and SDHA. Error bars denote means ± SD. *$P < 0.05$. IgG, immunoglobulin G; IP, immunoprecipitation.

DISCUSSION

AML is one of the most common acute leukemia in adults. Standard chemotherapy treatment for AML with 7 days of cytarabine followed by 3 days of anthracycline has been used for more 30 years, but the novel targeted therapies for AML are very limited (*32*). Despite the fact that reduction of leukemic cells can be achieved with conventional chemotherapy in most AML patients, disease relapse is not solved and the long-term outcomes of AML patients have not significantly improved. This is due to the fact that heterogeneous organization of AML contains a rare subpopulation of leukemia cells that are resistant to the present chemotherapy. The subset of resistant AML cells with dormancy and self-renewal properties could initiate and maintain the disease; thus, even a rare number of residual cells could drive disease relapse after chemotherapy (*33*). However, current strategies fail to specifically target leukemic cells and eliminate all chemotherapy-resistant cells. Accurately targeting and determining how leukemic cells behave in vivo have significant impact for the early diagnosis of leukemia, for monitoring treatment response, and for detecting how minimal residual leukemia cells lead to disease relapse after treatment (*34*). Techniques such as real-time qPCR or multiparameter flow cytometry have been used to assess specific malignant cells in AML and have been proven to positively affect the clinical decision-making for disease management, providing prognostic information for patient outcomes. These methods could not collect enough events at the right time to evaluate valid disease information because the residual leukemia cells are a rare population of cells. Furthermore, these strategies aim at specific genetic mutations in leukemia cells, such as FLT3, NPM1, DNMP3A, and IDH1/2 (*35*, *36*), to detect malignant cells. However, most AML patients do not present typical mutations because of the complexity of genomic mutation and the abnormal heterogeneity in different leukemia cells. Therefore, developing a new AML-targeting strategy based on the common vulnerability of malignant cells is urgently needed. In this study, the identified NIR fluorescence dye IR-26 is demonstrated to specifically target leukemia cells in vitro and in vivo based on the mechanism of hyperactive HIF-1α/glycolysis metabolism and increased SLC1B3 transporter's activity, which is similar to our previous studies in solid tumor targeting (*19*, *21*). Because aerobic glycolysis is known as the basic metabolic characteristic and an important hallmark of malignant cells, our studies may represent an entirely new AML-targeting strategy based on the common vulnerability of malignant cells. IR-26 also has an intrinsic NIR fluorescent property with the absorption and emission peak in the NIR region (700 to 900 nm). With advantages of low background interference and deep tissue penetration, the NIR fluorescence imaging has already been dedicated immense attention in tumor detection. We have established a dual-channel (GFP and NIR) fluorescence IVFC system to treat blood flow as natural sheath flow for identifying and quantifying specific cells in circulatory system without extracting blood samples (*28*). Using the IVFC system, the NIR fluorescence dye IR-26 is demonstrated to specifically detect and continuously monitor hematologic malignant cells in peripheral blood of transplanted AML mouse model in a noninvasive way. Thus, our studies may set out a new strategy with AML cell-specific targeting and detection to continuously monitor AML disease progression and treatment response, which will greatly help to prevent unnecessary delays in administering upfront therapy and improve treatment efficiency. Especially, IR-26 could continuously detect the rare population of residual leukemia cells to monitor disease relapse in a noninvasive way, which is of particular significance for AML clinical treatment.

Considering that the rare residual leukemia cells in the heterogeneous constitution of AML are demonstrated as the key factor responsible for chemotherapy resistance and disease relapse, identifying the common therapeutic vulnerability of chemotherapy-resistant leukemia cells should be important for AML therapy. Current studies have indicated that chemotherapy-resistant AML cells have unique mitochondrial characteristics of increased mitochondrial biogenesis and prevailingly dependent on OXPHOS for energy production and survival. Targeting the AML-specific alterations of mitochondria may emerge as intriguing targets for AML treatment strategies, especially for the chemotherapy-resistant AML or relapse of AML (*37*, *38*). The OXPHOS metabolic pathway is known to have a critical function in mitochondria by generating a sequential redox reaction within ETC pumping protons across the mitochondrial membrane to generate a gradient for ATP production. Thus, targeting the mitochondrial ETC complexes that directly affect the mitochondrial OXPHOS functions is definitely a theoretically potential target for tumor therapy. The anti-diabetic agent metformin, also known as an inhibitor of mitochondrial respiratory complex I, was evaluated in preclinical and clinical studies for solid tumor treatment and also showed promising results in AML treatment (*39*). The F_0F_1 ATP synthase inhibitor Gboxin was used to inhibit the growth of glioblastoma cells in a recent research (*40*). The inhibitor of complex I, IACS-010759, was identified as a clinical-grade small molecule for phase 1 clinical trials of relapsed/refractory AML, mantle cell lymphoma (MCL), and solid tumors (*13*). However, mitochondrion is the central checkpoint of cell metabolism, which is involved in energetic and biosynthetic processes for almost all cells; the integrity and functions of mitochondria are also comparably important for normal cells. Most of the present OXPHOS inhibitors are limited in anticancer therapy for the lack of tumor-targeting ability and potential severe side effects. Only Gboxin has been reported to accumulate in malignant cells depending on the high mitochondrial membrane potential and to exert cytotoxicity in glioblastoma (*40*). However, mitochondrial membrane potential is not the inherent characteristic of malignant cells and is much susceptible to many factors. In the study, we have characterized an AML-targeted dye, IR-26, that selectively accumulates in the mitochondria of AML cells based on the hyperactivity of HIF-1α/glycolysis, which is the common metabolic vulnerability and a hallmark of malignant cells. IR-26 robustly inhibited human leukemia cells in both OCR and galactose viability assay with similar IC_{50} values (average IC_{50} values were 3.632 and 2.913 μM; fig. S7), indicating that OXPHOS inhibition is an important mechanism for the anti-leukemia effect of IR-26 in human cells. IR-26 is also demonstrated to target the mitochondrial complex II protein SDHA and complex V protein ATP5B, decrease the functional activity of complexes II and V simultaneously to impair mitochondrial OXPHOS functions in AML cells, and exert targeted therapeutic effects in AML cells. In particular, IR-26 treatment has benefits for decreasing disease relapse and increasing the long-term survival in AML animal models. Therefore, the glycolysis-dependent OXPHOS inhibitor IR-26 may represent a new AML-targeted therapeutic strategy based on the common metabolic vulnerability of AML cells and may provide an opportunity for targeted killing of residual malignant cells by directly impairing mitochondrial OXPHOS functions.

In summary, our study reveals a new leukemia-targeted mechanism depending on the basic metabolic characteristic of hyperactive

glycolysis in AML cells and provides a rational AML therapeutic strategy by integrating simultaneous AML cells detection and targeted treatment. Continuous detection of AML cells in vivo helps to monitor the rare population of residual chemotherapy-resistant leukemia cell behaviors in patients, which may indicate an opportunity for reducing the disease relapse. The AML-targeted therapy based on mitochondrial OXPHOS inhibition has great advantages in selective killing of AML cells rather than normal cells to improve the treatment efficiency in AML without inducing obvious side effects. The multifunctional mitochondrial OXPHOS inhibitor IR-26 represents a new all-in-one agent for the integration of AML targeting, detection, and therapy, which may help to monitor disease progression and treatment responses and improve therapeutic efficiency to the residual cells that are responsible for disease relapse.

MATERIALS AND METHODS

Synthesis and characterization of IR-26

The synthetic route of compound IR-26 was shown in fig. S2. Compounds **2** and **4** were prepared according to the previously reported methods (*41*). Next, compound **5** was synthesized by an amidation reaction between compound **2** (2.12 g, 10 mmol) and compound **4** (1.25 g, 10 mmol) in the presence of triethylamine (Et_3N, 10 mmol) with a yield of 60%, white solid, and melting point of 51° to 52°C. ^1H nuclear magnetic resonance (NMR; 400 MHz, $CDCl_3$) δ: 1.49 (m, 2H), 1.69 (m, 2H), 1.86 (m, 2H), 2.27 (t, J = 7.5 Hz, 2H), 3.41 (t, J = 6.7 Hz, 2H), 3.77 (s, 3H), 4.06 (d, J = 5.1 Hz, 2H), 5.99 (s, 1H). Subsequently, alkylation reaction between 2,3,3-trimethyl-3*H* indole and **5** was carried out under 110°C for 10 hours in 1,2-dichlorobenzene to obtain compound **6** in the form of indole quaternary ammonium salt. Without purification of **6**, it was reacted with **7** (1.03 g, 6 mmol) by a condensation reaction in 40 ml of absolute ethanol solution of sodium acetate (0.49 g, 6 mmol) to finally synthesize IR-26 (1.63 g, yield 30%, green sticky solid). Structural characterization was determined by ^1H NMR, ^{13}C NMR, and high resolution mass spectroscopy (HRMS).

Cell lines and cell culture

Human leukemia cell lines HL-60, NB4, and THP-1 were cultured in RPMI 1640 culture media supplemented with 10% FBS. All cell lines were purchased from the American Type Culture Collection (Manassas, VA, USA) and incubated at 37°C with 5% CO_2. Lentiviral vector harboring the GFP gene was used to stably labeled HL-60 cells. The expression of GFP in antibiotic-resistant transfected cells was isolated by flow cytometry based on GFP fluorescence signals. HSCs were isolated from human cord blood with $CD34^+$ cells and cultured in serum-free medium with recombinant human stem cell factor (rhSCF), recombinant human thrombopoietin (rhTPO), and FLT3.

Detection of IR-26 accumulations in leukemia cells

To determine the preferential accumulation of IR-26 in leukemia cells, PBMCs from normal peripheral blood and different leukemia cells were incubated with 5 μM IR-26 at 37°C for 15 min. Cells were placed into a petri dish, and NIR fluorescence intensities were detected and compared by confocal microscopy (Leica) with 633-nm excitation and 780-nm emission. Moreover, GFP-labeled HL-60 cells were mixed with PBMCs and incubated with IR-26 at the same conditions. After washing with PBS, flow cytometry (BD FACSVerse, BD Biosciences) or confocal microscopy was used to determine the distribution of NIR fluorescence in GFP and non-GFP cells.

AML mouse models

Animal protocols were in accordance with the "Animal Care and Committee Guidelines of the Third Military Medical University." For the subcutaneous xenograft tumor models, male athymic nude mice (4 to 6 weeks old) were used. GFP-labeled HL-60 cells (5×10^6) were suspended in Dulbecco's minimum essential medium with the same volume of Matrigel (BD Biosciences) and subcutaneously injected into the flank of each mouse. For mouse model of human AML, male C57BL/6 mice (6 to 8 weeks old) were exposed to a sublethal irradiation at a dose of 6 Gy using a cobalt-60 source. GFP-labeled HL-60 cells (5×10^6) suspended in 300 μl of PBS were injected into mice through the tail vein. GFP-labeled malignant cells in peripheral blood were monitored by IVFC for 20 days, and leukemia blasts infiltrated in peripheral blood, bone marrow, spleens, and liver were detected to confirm that leukemia mouse models were established successfully. NOD/SCID mice engrafted with GFP-labeled human AML cells by tail vein injection were used to detect anti-leukemia efficacy of IR-26 in vivo.

In vivo and ex vivo optical imaging

Athymic nude mice bearing tumor xenografts were injected intravenously with IR-26 at a dose of 0.3 mg/kg (n = 3). Whole body of mouse optical imaging was taken at day 2 after injection using Kodak In-Vivo Imaging System FX Pro (New Haven, CT) equipped with fluorescent filter sets (excitation/emission, 770/830 nm); all settings were applied as described previously (*21*). After mice were sacrificed, dissected organs and tumors were obtained for NIR fluorescent imaging at the day of sacrifice.

IVFC detection

The NIR IVFC system used in this study was established by ourselves and equipped with two lasers: a 785-nm laser used to excite NIR fluorescent dyes, and a 488-nm laser used to excite GFP. Once a fluorescence cell in the blood passed through the laser slit, the fluorescence of both channels would be excited and detected at the same time. After the GFP-labeled leukemia cells were transplanted in the mice for 5 days, the mice were injected with IR-26 by tail vein. IVFC for tracking fluorescent cells in peripheral blood of mice was performed according to our previous protocols (*24*). Briefly, after the mouse was anesthetized with 1% sodium pentobarbital solution, it was placed on the platform, and the GFP and NIR fluorescence information in peripheral blood of mouse was recorded and analyzed using IVFC. The first measurements were acquired within 15 min after the first injection of IR-26. Additional measurements were acquired at the same vessel location.

In vivo anti-AML assays

To detect the anti-AML effects of IR-26 in vivo, xenograft tumor models, established by subcutaneous injection of HL-60 cells in the right flank of athymic nude mice (4 to 6 weeks old), were used. Drug treatment was started when tumor sizes reached 5 mm in diameter. The IR-26 treatment group (n = 5) received IR-26 (5.0 mg/kg) by intraperitoneal injection, and the cytarabine treatment group (n = 5) received cytarabine (50 mg/kg), whereas the control group (n = 5) received saline only. The compounds were injected three times a week. Tumor volumes were calculated as length × $(\text{width})^2/2$. NOD/SCID mice (8 to 10 weeks old) were intravenously injected with 5×10^6 GFP-labeled HL-60 cells to establish human AML mouse model. The mice were kept in microisolators and fed with sterile food and acidified water. One week after injection of HL-60 cells, the IR-26

treatment group ($n = 12$) received IR-26 (5.0 mg/kg) in saline by intraperitoneal injection, and the cytarabine treatment group ($n = 12$) was intraperitoneally injected with cytarabine (5.0 mg/kg), whereas the control group ($n = 12$) received saline only. Leukemia cell distribution, pathological histology of vital organs, and mice survival rates were detected.

Seahorse XF assays

Cellular OCR was measured using XF96 Extracellular Flux Analyzer (Seahorse Bioscience, Billerica, MA). Briefly, HL-60 cells were seeded in XF96-well plates (20,000 cells per well in 80 μl). After 1 hour, cells were incubated overnight at 37°C, 5% CO_2. The XF96 sensor cartridge was hydrated with 200 μl of calibration buffer per well overnight at 37°C. Cells were preincubated with or without IR-34 (5 μM) for 1 hour before the bioenergetic profile was determined. Then, cells were washed twice with 200 μl of prewarmed base medium containing 10 mM sodium pyruvate and 25 mM glucose. The sensor cartridge was loaded with assay media (ports A, B, and C) to measure basal OCR or with oligomycin (2.0 μM, port A), carbonyl cyanide 4-(trifluoromethoxy) phenylhydrazone (2.0 μM, port B), and rotenone (0.5 μM, port C) to measure the bioenergetic profiles of different cells.

Pull-down experiment assay

Pull-down assay using IR-26–labeled AML cells were performed to detect IR-26–specific interaction proteins. Briefly, HL-60 cells were incubated with 1.25 μM IR-26 for 15 min. After washing with PBS, the cells were lysed to obtain the total protein. Then, the protein lysate was incubated with SDHA and ATP5B antibodies overnight at 4°C. A total of 100 μl of streptavidin-agarose (Santa Cruz Biotechnology) was added and incubated for 2 hours at room temperature, and the immunoglobulin G antibody was used as control. After the protein complex was centrifuged and washed, it was analyzed by SDS–polyacrylamide gel electrophoresis and imaging using Kodak In-Vivo Imaging System FX Pro to determine whether ATP5B or SDHA proteins were combined with the NIR fluorescence small-molecule IR-26 and then immunoblotted using anti-ATP5B or anti-SDHA antibodies to further verify the interactions.

Metabolomic analysis

The HL-60 cells were cultured in RPMI 1640 culture media supplemented with 10% FBS for 2 days. Next, 1×10^7 cells were seeded in 75 culture dishes and treated with different concentrations of IR-26 (0, 2.5, 5, and 10 μM). After 8 hours, cells in different groups were harvested and counted. After centrifugation, cells were kept in liquid nitrogen for 30 s and stored under −80°C condition. Then, metabolites were immediately extracted and subjected to targeted metabolomic analysis for central carbon metabolism. Electrospray ionization mass spectrometry (cation) or Agilent 6460 Triple Quad LC/MS (anion) was conducted by Biotree.

Statistical analyses

Data were presented as means ± SD from at least three independent experiments. SPSS 13.0 statistical software was used to conduct all statistical analysis. One-way analysis of variance was used to determine significance among groups. A value of $P < 0.05$ was considered to be statistically significant.

SUPPLEMENTARY MATERIALS

Supplementary material for this article is available at http://advances.sciencemag.org/cgi/content/full/7/1/eabb6104/DC1

View/request a protocol for this paper from *Bio-protocol*.

REFERENCES AND NOTES

1. H. Döhner, D. J. Weisdorf, C. D. Bloomfield, Acute myeloid leukemia. *N. Engl. J. Med.* **373**, 1136–1152 (2015).
2. A. Khwaja, M. Bjorkholm, R. E. Gale, R. L. Levine, C. T. Jordan, G. Ehninger, C. D. Bloomfield, E. Estey, A. Burnett, J. J. Cornelissen, D. A. Scheinberg, D. Bouscary, D. C. Linch, Acute myeloid leukaemia. *Nat. Rev. Dis. Primers.* **2**, 16010 (2016).
3. C. S. Hourigan, J. E. Karp, Minimal residual disease in acute myeloid leukaemia. *Nat. Rev. Clin. Oncol.* **10**, 460–471 (2013).
4. L. I. Shlush, A. Mitchell, L. Heisler, S. Abelson, S. W. K. Ng, A. Trotman-Grant, J. J. F. Medeiros, A. Rao-Bhatia, I. Jaciw-Zurakowsky, R. Marke, J. L. McLeod, M. Doedens, G. Bader, V. Voisin, C. Xu, J. D. McPherson, T. J. Hudson, J. C. Y. Wang, M. D. Minden, J. E. Dick, Tracing the origins of relapse in acute myeloid leukaemia to stem cells. *Nature* **547**, 104–108 (2017).
5. C. C. Smith, A. Paguirigan, G. R. Jeschke, K. C. Lin, E. Massi, T. Tarver, C. S. Chin, S. Asthana, A. Olshen, K. J. Travers, S. Wang, M. J. Levis, A. E. Perl, J. P. Radich, N. P. Shah, Heterogeneous resistance to quizartinib in acute myeloid leukemia revealed by single-cell analysis. *Blood* **130**, 48–58 (2017).
6. Y. Chen, J. Hu, Nucleophosmin1 (NPM1) abnormality in hematologic malignancies, and therapeutic targeting of mutant NPM1 in acute myeloid leukemia. *Ther. Adv. Hematol.* **11**, 2040620719899818 (2020).
7. C. C. Coombs, M. S. Tallman, R. L. Levine, Molecular therapy for acute myeloid leukaemia. *Nat. Rev. Clin. Oncol.ss* **13**, 305–318 (2016).
8. J. A. Martignoles, F. Delhommeau, P. Hirsch, Genetic hierarchy of acute myeloid leukemia: From clonal hematopoiesis to molecular residual disease. *Int. J. Mol. Sci.* **19**, 3850 (2018).
9. A. Kohlmann, N. Nadarajah, T. Alpermann, V. Grossmann, S. Schindela, F. Dicker, A. Roller, W. Kern, C. Haferlach, S. Schnittger, T. Haferlach, Monitoring of residual disease by next-generation deep-sequencing of *RUNX1* mutations can identify acute myeloid leukemia patients with resistant disease. *Leukemia* **28**, 129–137 (2014).
10. F. Pastore, R. L. Levine, Next-generation sequencing and detection of minimal residual disease in acute myeloid leukemia: Ready for clinical practice? *JAMA* **314**, 778–780 (2015).
11. R. J. DeBerardinis, N. S. Chandel, Fundamentals of cancer metabolism. *Sci. Adv.* **2**, e1600200 (2016).
12. M. Rashkovan, A. Ferrando, Metabolic dependencies and vulnerabilities in leukemia. *Gene Dev.* **33**, 1460–1474 (2019).
13. J. R. Molina, Y. Sun, M. Protopopova, S. Gera, M. Bandi, C. Bristow, T. McAfoos, P. Morlacchi, J. Ackroyd, A. A. Agip, G. Al-Atrash, J. Asara, J. Bardenhagen, C. C. Carrillo, C. Carroll, E. Chang, S. Ciurea, J. B. Cross, B. Czako, A. Deem, N. Daver, J. F. de Groot, J. -W. Dong, N. Feng, G. Gao, J. Gay, M. G. Do, J. Greer, V. Giuliani, J. Han, L. Han, V. K. Henry, J. Hirst, S. Huang, Y. Jiang, Z. Kang, T. Khor, S. Konoplev, Y.-H. Lin, G. Liu, A. Lodi, T. Lofton, H. Ma, M. Mahendra, P. Matre, R. Mullinax, M. Peoples, A. Petrocchi, J. Rodriguez-Canale, R. Serreli, T. Shi, M. Smith, Y. Tabe, J. Theroff, S. Tiziani, Q. Xu, Q. Zhang, F. Muller, R. A. DePinho, C. Toniatti, G. F. Draetta, T. P. Heffernan, M. Konopleva, P. Jones, M. E. Di Francesco, J. R. Marszalek, An inhibitor of oxidative phosphorylation exploits cancer vulnerability. *Nat. Med.* **24**, 1036–1046 (2018).
14. T. Farge, E. Saland, F. de Toni, N. Aroua, M. Hosseini, R. Perry, C. Bosc, M. Sugita, L. Stuani, M. Fraisse, S. Scotland, C. Larrue, H. Boutzen, V. Féliu, M.-L. Nicolau-Travers, S. Cassant-Sourdy, N. Broin, M. David, N. Serhan, A. Sarry, S. Tavitian, T. Kaoma, L. Vallar, J. Iacovoni, L. K. Linares, C. Montersino, R. Castellano, E. Griessinger, Y. Collette, O. Duchamp, Y. Barreira, P. Hirsch, T. Palama, L. Gales, F. Delhommeau, B. H. Garmy-Susini, J.-C. Portais, F. Vergez, M. Selak, G. Danet-Desnoyers, M. Carroll, C. Récher, J.-E. Sarry, Chemotherapy-resistant human acute myeloid leukemia cells are not enriched for leukemic stem cells but require oxidative metabolism. *Cancer Discov.* **7**, 716–735 (2017).
15. I. Baccelli, Y. Gareau, B. Lehnertz, S. Gingras, J.-F. Spinella, S. Corneau, N. Mayotte, S. Girard, M. Frechette, V. Blouin-Chagnon, K. Leveillé, I. Boivin, T. MacRae, J. Krosl, C. Thiollier, V.-P. Lavallée, E. Kanshin, T. Bertomeu, J. Coulombe-Huntington, C. St-Denis, M.-E. Bordeleau, G. Boucher, P. P. Roux, S. Lemieux, M. Tyers, P. Thibault, J. Hébert, A. Marinier, G. Sauvageau, Mubritinib targets the electron transport chain complex I and reveals the landscape of OXPHOS dependency in acute myeloid leukemia. *Cancer Cell* **36**, 84–99 (2019).
16. L. Zhang, Y. Yao, S. Zhang, Y. Liu, H. Guo, M. Ahmed, T. Bell, H. Zhang, G. Han, E. Lorence, M. Badillo, S. Zhou, Y. Sun, M. E. Di Francesco, N. Feng, R. Haun, R. Lan, S. G. Mackintosh, X. Mao, X. Song, J. Zhang, L. V. Pham, P. L. Lorenzi, J. Marszalek, T. Heffernan, G. Draetta, P. Jones, A. Futreal, K. Nomie, L. Wang, M. Wang, Metabolic reprogramming toward oxidative phosphorylation identifies a therapeutic target for mantle cell lymphoma. *Sci. Transl. Med.* **11**, eaau1167 (2019).
17. H. R. Bridges, A. J. Jones, M. N. Pollak, J. Hirst, Effects of metformin and other biguanides on oxidative phosphorylation in mitochondria. *Biochem. J.* **462**, 475–487 (2014).
18. G. Cheng, J. Zielonka, O. Ouari, M. Lopez, D. M. Allister, K. Boyle, C. S. Barrios, J. J. Weber, B. D. Johnson, M. Hardy, M. B. Dwinell, B. Kalyanaraman, Mitochondria-targeted analogues of metformin exhibit enhanced antiproliferative and radiosensitizing effects in pancreatic cancer cells. *Cancer Res.* **76**, 3904–3915 (2016).

19. E. Iglesias, A. Pesini, N. Garrido-Pérez, P. Meade, M. P. Bayona-Bafaluy, J. Montoya, E. Ruiz-Pesini, Prenatal exposure to oxidative phosphorylation xenobiotics and late-onset Parkinson disease. *Ageing Res. Rev.* **45**, 24–32 (2018).
20. V. Sica, J. M. Bravo-San Pedro, G. Stoll, G. Kroemer, Oxidative phosphorylation as a potential therapeutic target for cancer therapy. *Int. J. Cancer* **146**, 10–17 (2020).
21. C. Zhang, T. Liu, Y. Su, S. Luo, Y. Zhu, X. Tan, S. Fan, L. Zhang, Y. Zhou, T. Cheng, C. Shi, A near-infrared fluorescent heptamethine indocyanine dye with preferential tumor accumulation for in vivo imaging. *Biomaterials* **31**, 6612–6617 (2010).
22. S. Luo, E. Zhang, Y. Su, T. Cheng, C. Shi, A review of NIR dyes in cancer targeting and imaging. *Biomaterials* **32**, 7127–7138 (2011).
23. E. L. Zhang, S. L. Luo, X. Tan, C. M. Shi, Mechanistic study of IR-780 dye as a potential tumor targeting and drug delivery agent. *Biomaterials* **35**, 771–778 (2014).
24. J. B. Wu, C. Shao, X. Li, C. Shi, Q. Li, P. Hu, Y.-T. Chen, X. Dou, D. Sahu, W. Li, H. Harada, Y. Zhang, R. Wang, H. E. Zhau, L. W. Chung, Near-infrared fluorescence imaging of cancer mediated by tumor hypoxia and HIF1α/OATPs signaling axis. *Biomaterials* **35**, 8175–8185 (2014).
25. Y. Wang, X. Y. Liao, J. G. Sun, B. Yi, S. L. Luo, T. Liu, X. Tan, D. Q. Liu, Z. L. Chen, X. Wang, C. M. Shi, Characterization of HIF-1α/glycolysis hyperactive cell population via small-molecule-based imaging of mitochondrial transporter activity. *Adv. Sci.* **5**, 1700392 (2018).
26. A. L. Vahrmeijer, M. Hutteman, J. R. van der Vorst, C. J. H. van de Velde, J. V. Frangioni, Image-guided cancer surgery using near-infrared fluorescence. *Nat. Rev. Clin. Oncol.* **10**, 507–518 (2013).
27. A. L. Antaris, H. Chen, K. Cheng, Y. Sun, G. Hong, C. Qu, S. Diao, Z. Deng, X. Hu, B. Zhang, X. Zhang, O. K. Yaghi, Z. R. Alamparambil, X. Hong, Z. Cheng, H. Dai, A small-molecule dye for NIR-II imaging. *Nat. Mater.* **15**, 235 (2016).
28. Y. Suo, T. Liu, C. Xie, D. Wei, X. Tan, L. Wu, X. Wang, H. He, G. Shi, X. Wei, C. Shi, Near infrared in vivo flow cytometry for tracking fluorescent circulating cells. *Cytometry A* **87**, 878–884 (2015).
29. S. Luo, X. Tan, S. Fang, Y. Wang, T. Liu, X. Wang, Y. Yuan, H. Sun, Q. Qi, C. Shi, Mitochondria-targeted small-molecule fluorophores for dual modal cancer phototherapy. *Adv. Funct. Mater.* **26**, 2826–2835 (2016).
30. X. Tan, S. Luo, L. Long, Y. Wang, D. Wang, S. Fang, Q. Ouyang, Y. Su, T. Cheng, C. Shi, Structure-guided design and synthesis of a mitochondria-targeting near-infrared fluorophore with multimodal therapeutic activities. *Adv. Mater.* **29**, 1704196 (2017).
31. Y. Wang, S. Luo, C. Zhang, X. Liao, T. Liu, Z. Jiang, D. Liu, X. Tan, L. Long, Y. Wang, Z. Chen, Y. Liu, F. Yang, Y. Gan, C. Shi, An NIR-fluorophore-based therapeutic endoplasmic reticulum stress inducer. *Adv. Mater.* , e1800475 (2018).
32. D. Vetrie, G. V. Helgason, M. Copland, The leukaemia stem cell: Similarities, differences and clinical prospects in CML and AML. *Nat. Rev. Cancer* **20**, 158–173 (2020).
33. A. L. Boyd, L. Aslostovar, J. Reid, W. Ye, B. Tanasijevic, D. P. Porras, Z. Shapovalova, M. Almakadi, R. Foley, B. Leber, A. Xenocostas, M. Bhatia, Identification of chemotherapy-induced leukemic-regenerating cells reveals a transient vulnerability of human AML recurrence. *Cancer Cell* **34**, 483–498.e5 (2018).
34. F. Lassailly, E. Griessinger, D. Bonnet, "Microenvironmental contaminations" induced by fluorescent lipophilic dyes used for noninvasive in vitro and in vivo cell tracking. *Blood* **115**, 5347–5354 (2010).
35. B. A. Carneiro, J. K. Altman, J. B. Kaplan, G. Ossenkoppele, R. Swords, L. C. Platanias, F. J. Giles, Targeted therapy of acute myeloid leukemia. *Expert Rev. Anticancer Ther.* **15**, 399–413 (2015).
36. E. M. Stein, Molecularly targeted therapies for acute myeloid leukemia. *Hematology Am. Soc. Hematol. Educ. Program* **2015**, 579–583 (2015).
37. S. Bhatt, H. Zhu, D. Weinstock, J. Garcia, A. Letai, Probing mitochondria to guide personalized therapy for acute myeloid leukemia. *Clin. Cancer Res.* **23**, 34–35 (2017).
38. E. A. Lee, L. Angka, S. G. Rota, T. Hanlon, A. Mitchell, R. Hurren, X. M. Wang, M. Gronda, E. Boyaci, B. Bojko, M. Minden, S. Sriskanthadevan, A. Datti, J. L. Wrana, A. Edginton, J. Pawliszyn, J. W. Joseph, J. Quadrilatero, A. D. Schimmer, P. A. Spagnuolo, Targeting mitochondria with avocatin B induces selective leukemia cell death. *Cancer Res.* **75**, 2478–2488 (2015).
39. S. Scotland, E. Saland, N. Skuli, F. de Toni, H. Boutzen, E. Micklow, I. Sénégas, R. Peyraud, L. Peyriga, F. Théodoro, E. Dumon, Y. Martineau, G. Danet-Desnoyers, F. Bono, C. Rocher, T. Levade, S. Manenti, C. Junot, J.-C. Portais, N. Alet, C. Recher, M. A. Selak, M. Carroll, J.-E. Sarry, Mitochondrial energetic and AKT status mediate metabolic effects and apoptosis of metformin in human leukemic cells. *Leukemia* **27**, 2129–2138 (2013).
40. Y. Shi, S. K. Lim, Q. Liang, S. V. Iyer, H.-Y. Wang, Z. Wang, X. Xie, D. Sun, Y.-J. Chen, V. Tabar, P. Gutin, N. Williams, J. K. De Brabander, L. F. Parada, Gboxin is an oxidative phosphorylation inhibitor that targets glioblastoma. *Nature* **567**, 341–346 (2019).
41. T. C. Preston, M. Nuruzzaman, N. D. Jones, S. Mittler, Role of hydrogen bonding in the pH-dependent aggregation of colloidal gold particles bearing solution-facing carboxylic acid groups. *J. Phys. Chem. C* **113**, 14236–14244 (2009).

Acknowledgments

Funding: This work was supported by Natural Science Foundation Programs (81130026 and 81773352), Innovation Team Building Program of Chongqing University (CXTDG201602020), and Outstanding Youth Development Program of Third Military Medical University. **Author contributions:** C.Z., Yang Wang, T.L., and P.L. performed experiments. L.G. collected patient samples. L.M., Z.J., and Z.Y. helped to perform in vitro experiments. D.L., X.L., and Q.J. helped to perform in vivo experiments. X.T. and Yu Wang helped with optical imaging. S.L. contributed to design and synthesis of compounds and preparation of the manuscript. Yang Wang and C.S. contributed to study design, manuscript writing, and project supervision. **Competing interests:** The authors declare that they have no competing interests. **Data and materials availability:** All data needed to evaluate the conclusions in the paper are present in the paper and/or the Supplementary Materials. Additional data related to this paper may be requested from the authors.

Submitted 6 March 2020
Accepted 4 November 2020
Published 1 January 2021
10.1126/sciadv.abb6104

Citation: C. Zhang, T. Liu, P. Luo, L. Gao, X. Liao, L. Ma, Z. Jiang, D. Liu, Z. Yang, Q. Jiang, Y. Wang, X. Tan, S. Luo, Y. Wang, C. Shi, Near-infrared oxidative phosphorylation inhibitor integrates acute myeloid leukemia–targeted imaging and therapy. *Sci. Adv.* **7**, eabb6104 (2021).